DMT Modulation with Adaptive Loading for High Bit Rate Transmission Over Directly Detected Optical Channels

Laia Nadal, Michela Svaluto Moreolo, *Senior Member, IEEE*, Josep M. Fàbrega, *Member, IEEE*, Annika Dochhan *Member, IEEE*, Helmut Grießer, *Member, IEEE*, Michael Eiselt, *Senior Member, IEEE*, and Jörg-Peter Elbers, *Member, IEEE*

***Abstract*—In this paper, we present the design and analysis of an adaptive cost-effective discrete multitone (DMT) transponder using direct detection (DD) suitable for data center interconnections. Levin Campello margin adaptive (LC-MA) algorithm is applied to the transponder digital signal processing (DSP) modules to enhance fiber chromatic dispersion (CD) resilience, while achieving high data rate transmission. The bit error rate (BER) performance and the rate/distance adaptive capabilities of the proposed transponder have been numerically analyzed and compared to bandwidth variable uniform loading, taking into account the transmission impairments at the varying of the fiber length. Specifically, the performance of the designed transponder has been assessed from 20 Gb/s to 112 Gb/s, extending the achievable reach at 50 Gb/s beyond 80 km of standard single mode fiber (SSMF). The numerical simulations have been compared with experimental results, evidencing good agreement in presence of transmission impairments.**

***Index Terms*—Bit loading, power loading, DD, DMT, optical communications.**

I. Introduction

INTRA or short inter data center point-to-point fiber optics interfaces are defined as client optics. Major client optics applications can be general data center and metro inter data center connections which typically cover distances from 10 km up to 40 km of standard single mode fiber (SSMF) [1]. According to a recent study of Cisco in [2], the global data center and cloud IP traffic is increasing drastically every month. In order to allow connectivity for these high volumes of data between data centers, an increased transmission capacity and high data rates client interfaces should be achieved which support 100 Gb/s transmission per lane [3]. Hence, at the data plane level, innovative transceivers based on optical orthogonal frequency division multiplexing (O-OFDM) formats are under investigation in order to support high channel rates and enhance the transmission capacity and the spectral efficiency of the software-defined transmission [4], [5]. However, as a high number of links are required to interconnect all the data centers distributed over an area, the cost and simplicity of the optical implementation of transponders are still key issues. Thus, direct detection (DD) optical OFDM is considered for cost-effective applications that uses simple transmitter and receiver architectures [6], [7]. More specifically, discrete multitone modulation (DMT) can be used in DD optical systems to create real-valued OFDM symbols simplifying their implementation [8]. The signal processing in the DMT transmitter/receiver is based on the fast Fourier transform (FFT), forcing the Hermitian symmetry (HS) on the input symbols. Alternative transforms to the FFT can also be used to implement the DMT symbols [9].

The electrical-to-optical conversion in DMT systems can be implemented by directly or externally modulating the DMT signal. On one hand, directly modulated lasers (DML) provide high output power and low threshold current [10]. DML is a low cost solution, but it introduces high laser chirp, limiting the transmission reach and the achievable bit rate. On the other hand, Mach-Zehnder modulators (MZM) externally modulate the DMT signal presenting negligible chirp. Thus, the required optical signal-to-noise ratio (OSNR), to ensure a target bit error rate (BER) and a certain transmission reach, is lower.

Despite the simplicity of DMT systems for short range applications, they are severely affected by fiber dispersion when operating at high bit rates, which introduces strong frequency selective fading [11]. Additional issues are related to the total electrical signal bandwidth occupancy (B_s), which is required to achieve high data rate. Specifically, the limited bandwidth of some electrical components such as the digital-to-analog converters (DAC) and analog-to-digital converters (ADC) can degrade the overall system performance.

A possible solution to enhance resilience towards system impairments and increase system capacity for high volume of inter data center traffic is bit loading (BL) and power loading (PL). BL and PL introduce flexibility in the system and robustness against transmission impairments by allocating different number of bits and power to the subcarriers according to the channel profile [12]. Different loading algorithms have been proposed in the literature for DMT systems to overcome chromatic dispersion (CD) and enhance the system performance (see e.g. [12] and [13]). These algorithms can be implemented considering different criteria: (i) BER minimization for fixed data rate and transmit power constraints,

This work was funded by the MINECO (Economy and competitiveness Ministry of Spain) through the project FARO (TEC2012-38119), FP7 EU-Japan project STRAUSS (GA 608528), and the FPI research scholarship grants BES-2010-031072 and EEBB-I-13-06102.

L. Nadal, M. Svaluto Moreolo and J.M. Fàbrega are with the Centre Tecnològic de Telecomunicacions de Catalunya, 08860 Castelldefels (Barcelona), Spain. (e-mail: laia.nadal@cttc.es).

H.Grießer and J.P. Elbers with ADVA Optical Networking SE, Fraunhoferstrasse 9a, 82152 Martinsried, Germany

A. Dochhan and M.Eiselt are with ADVA Optical Networking SE, Maerzenquelle 1-3, 98617 Meiningen, Germany.

(ii) Rate maximization for a fixed energy constraint and (iii) Energy minimization at a given data rate [12]. A loading algorithm addressing the problem of BER minimization is proposed in [14]. Cases (ii) and (iii) are usually referred to as rate adaptive (RA) and margin adaptive (MA) problems, respectively. A well-known algorithm that solves the RA and MA problems is the water-filling [15]. Since the related optimization problems are convex, the water-filling algorithm computes a global optimal solution (i.e. the minimum of the convex function). However, this algorithm assumes Gaussian symbol distribution, which implies considering infinite granularity in constellation sizes. Hence, a direct implementation in an actual system is not feasible. Alternatively, the Chow Cioffi Bingham (CCB) algorithm is proposed as a discrete loading solution that solves RA and MA optimization problems, assuming integer values for the number of bits assigned to each subcarrier. Specifically, the CCB algorithm, applied to RA and MA problems (CCB-RA and CCB-MA, respectively), arrives to a suboptimal solution by rounding the approximated water-filling results [12]. Another discrete loading approach is based on Levin Campello (LC) algorithm, which solves RA and MA problems (LC-RA and LC-MA, respectively) using greedy methods. Unlike the suboptimal CCB approach, LC algorithm finds a local optimal solution, as shown in [12] for a linear intersymbol interference / additive white Gaussian noise (ISI/AWGN) channel.

Several DMT systems, that can be applied in data center scenarios, are found in the literature. In [7], a detailed study by means of simulation is performed comparing various DMT systems with optimized BL and PL transmitting at 10.7 Gb/s. In [16], an experimental demonstration of the transmission of a DMT system using LC algorithm is performed. 19 Gb/s and 9.7 Gb/s are achieved over 25 km and 100 km, respectively. A later study shows a 50 Gb/s transmission over 20 km of SSMF with a DML laser and suboptimal bit and power loading [17]. In [18], 100 Gb/s transmission using suboptimal BL and PL is achieved after 10 km SSMF using a DML.

This paper provides the design and analysis of a high data rate adaptive DMT transponder using a DD optical implementation based on MZM featured with LC-MA. Specifically, the LC-MA algorithm is selected to be implemented in the transponder digital signal processing (DSP), as it is shown that this loading strategy outperforms the CCB loading algorithm [12]. A baseband signal is transmitted allowing a simpler implementation when comparing with other transmission systems such as single side band (SSB) modulation where optical filters or other complex schemes are needed [19]. The system performance is assessed by means of simulation at different data rates ranging from 20 Gb/s to 112 Gb/s. LC strategy is presented to overcome the CD and compared with CCB and uniform loading in which the signal bandwidth is adapted to the optical link. Additionally, the achieved numerical results are compared with the experimental results obtained in our previous publication [20], where data rates higher than 56 Gb/s are experimentally investigated. OSNR measurements have been performed, analyzing links of 50 km and 80 km, beyond the distances found in the literature. We demonstrate that using the presented design guidelines, the proposed adaptive transponder can be adopted as a solution for major client optics applications, providing a possible extension of the link reach between data centers.

The paper is organized as follows. In section II, the DMT transponder design is described, giving the guidelines for the fundamental DSP blocks implementation. In section III, simulation results are presented by first analyzing the system limitations. Then, it is shown that LC-MA presents superior performance compared to suboptimal loading such as the CCB. Finally, the BER performance and the achievable reach of the proposed system is investigated, evidencing the improvement over bandwidth variable uniform loading and taking into account the channel response and transmission impairments. In section IV, the experimental validation of the DMT system using LC-MA algorithm [20] is compared with the numerical analysis. The back-to-back (B2B) configuration and optical links of 50.5 km and 82.1 km of SSMF are investigated. Finally, conclusions are drawn in section V.

II. DMT TRANSPONDER DESIGN

Fig. 1 shows the system model of the proposed adaptive DMT transponder. The input data are parallelized and mapped onto the subcarriers using the same modulation format (uniform bit loading) or different formats per subcarrier (bit loading). Binary phase-shift keying (BPSK) and M-ary quadrature amplitude modulation (M QAM) are considered. The constellations of the analyzed formats have been implemented according to [21] and are indicated in Fig. 2. Then, training symbols (TS) are added for synchronization and channel estimation in reception. The resulting signal is fed into an N points inverse Fourier transform (IFFT), forcing HS to create the DMT symbols. At the increase of N, a finer granularity can be obtained, as a larger number of subcarriers can be mapped with different modulation formats. Thus, the system flexibility is enhanced. Then a cyclic prefix (CP) is added to cope with channel dispersion-induced ISI and inter-carrier interference (ICI). The CP must be chosen considering a trade-off between system performance and CP overhead [22]. However, when the DMT symbol size increases, the impact of CP overhead on the data rate is reduced. Additionally, symmetrical clipping is performed to limit the high peaks of power that can occur in the generation of a DMT signal, normally referred to as peak-to-average power ratio (PAPR) [23]. Clipping the signal results in clipping noise that degrades the DMT system performance; a detailed analysis is provided in [24]. The clipping level (C) is defined in decibels as

$$C = 10 \cdot \log_{10}\left(\frac{B^2}{E[|x_m|^2]}\right), \tag{1}$$

where x_m is the transmitted discrete signal, before clipping, $E[|x_m|^2]$ denotes the average signal power of the transmitted signal and B is the maximum allowed signal amplitude [23]. The clipping level must be selected according to the highest modulation format, in order to limit the clipping noise at the expense of increasing the power of the signal [25]. The serialized data are digital-to-analog converted with a DAC and modulated onto the optical carrier by means of a MZM. External modulation is used, in contrast to alternative

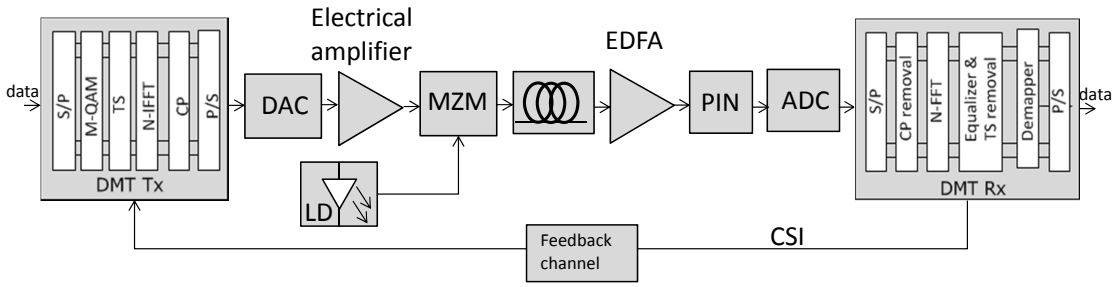

Fig. 1. DMT system model. The DSP modules at the DMT transmitter/receiver (Tx/Rx) are detailed.

implementations based on direct laser modulation, such as [16], where the DMT signal is directly modulated with a distributed feedback (DFB) laser. Then, the optical signal is transmitted over the fiber channel. CD limits the system performance when transmitting over the fiber. SSMF or other optical fibers with lower dispersion coefficients such as non-zero dispersion-shifted fiber (NZDSF) can be used as optical channel. Nevertheless, SSMF is considered for our analysis as it is the most critical case in terms of CD impact and it is deployed in most of major client optics applications [1]. According to [7], the n-th attenuation peak due to CD (being n any positive integer), appears at the frequency

$$f_{CD}^{n} = \sqrt{\frac{c(2n-1)/2\lambda^2}{LD}}, \tag{2}$$

where D is the dispersion coefficient parameter, L is the fiber length, λ is the center wavelength and c the speed of light. For a given fiber length, depending on the D value, the first peak at f_{CD}^{1} can fall out the bandwidth of interest. Using NZDSF, the frequency f_{CD}^{1} at which appears the first attenuation peak will be higher than the frequency f_{CD}^{1} in case of using SSMF.

At the receiver side, the DMT signal is detected with a PIN photodiode whereas in [16] an avalanche photodiode (APD) is used as PON is the target application. Then, the resulting signal is analog-to-digital converted and synchronized. Specifically, Schmidl & Cox's algorithm is generally used to perform the synchronization process [26]. This algorithm finds an approximation of the starting point of the OFDM symbol by using a TS in which the first half is identical to the second half in the time domain. For our design, a variation of this algorithm has been implemented transmitting two identical TS to estimate the beginning of the OFDM symbol. This way, these TS can also be used to perform the equalization processing. A timing metric, as defined in [26], is calculated, which reaches a plateau with length equal to the difference between the length of the cyclic prefix and the length of the channel impulse response. An average windowing is used to create a peak at the medium point of the plateau, which is selected as the start of the symbol. Finally, the signal is demodulated, equalized, and demapped. In order to implement the equalization, a diagonal matrix is constructed with the estimated channel coefficients, which result from the average quotient between the TS and the equivalent received symbols. From this first step equalization, the equalized data is used as input for a second step equalization, enabling decision directed

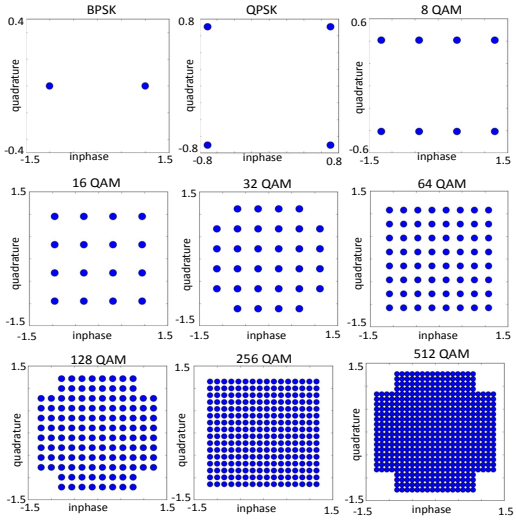

Fig. 2. BPSK and rectangular QAM constellations implemented at the transmitter [21].

channel estimation. Specifically, it consists of improving data decisions, by performing channel estimation using all the symbols [6]. Hence, the equalization matrix is updated and it can be used to retrieve the transmitted data.

An initial channel estimation can be performed by transmitting a probe DMT signal mapped with uniform loading. The signal-to-noise ratio (SNR) of each subcarrier is estimated at the receiver side and sent back to the transmitter as channel state information (CSI) through the feedback channel (see Fig.1) [6]. The feedback channel can be realized over the inverse channel of a bidirectional system setup (with usually a pair of fibers, but also a single fiber is possible). Also an optical supervisory channel (OSC), which is a dedicated low rate optical channel at a different wavelength can be used as it is present in many systems. The CSI is used to implement the LC-MA loading algorithm at the transmitter side. Specifically, LC-MA consists of finding the bit and power allocation for each subcarrier according to the channel profile for a fixed bit rate [12]. The basic concept of this iterative algorithm is that each increment of information is placed onto the subcarrier that requires less incremental energy for its transmission. In order to solve the MA problem, the LC algorithm finds an efficient symbol distribution by performing an exhaustive search [12]. The resulting bit distribution is defined as efficient when

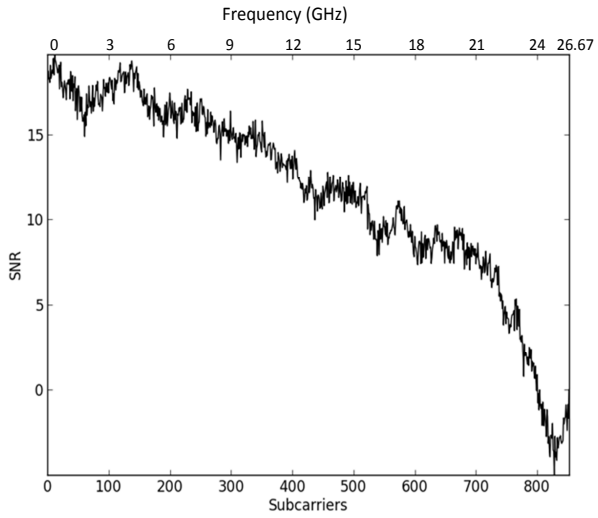

(a)

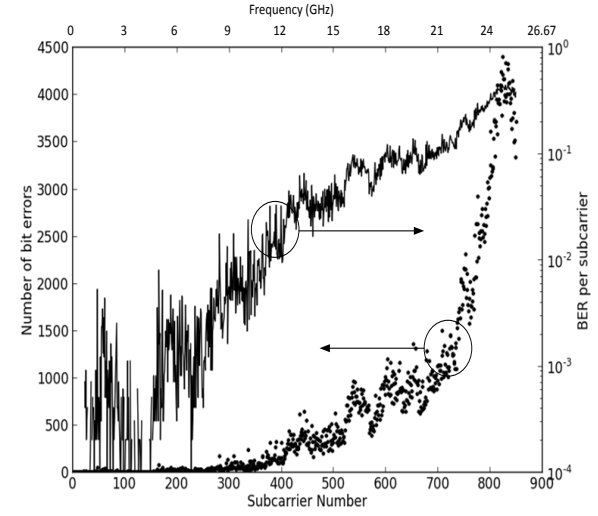

(b)

Fig. 3. (a) SNR estimation of an optical B2B channel and (b) BER (solid line) and number of errors (dotted line) per subcarrier transmitting 8441920 bits at 100 Gb/s with 16 QAM (Uniform bit loading) in the B2B configuration.

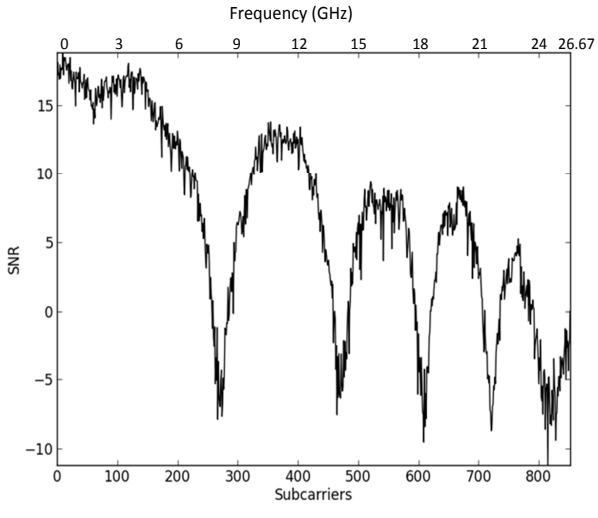

(a)

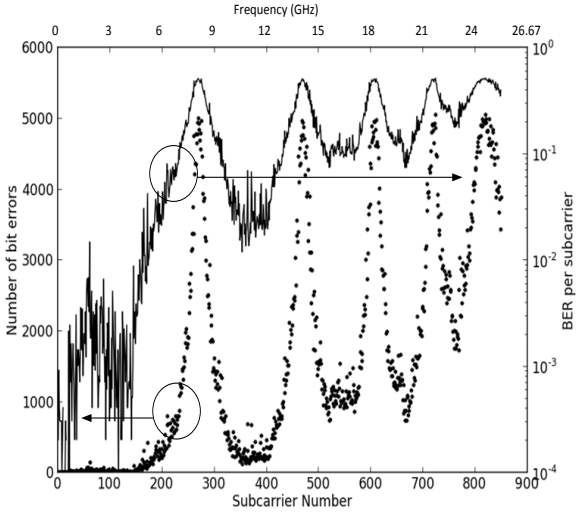

(b)

Fig. 4. (a) SNR estimation after 50 km of SSMF fiber and (b) BER (solid line) and number of errors (dotted line) per subcarrier transmitting 8441920 bits at 100 Gb/s with 16 QAM (Uniform bit loading) after 50 km of SSMF fiber.

the energy cannot be further reduced by any other loading scheme. Finally, the algorithm verifies that the correct number of bits is transmitted according to the target data rate, giving a local optimal solution. The gap approximation of the SNR, Γ, is used in order to relate the number of bits per symbol and the required SNR to achieve a target error probability in a straightforward manner, simplifying the bit loading algorithm [12]. In particular, according to [27], an initial value of $\Gamma = 9.8$ dB is used to calculate the energy of each subcarrier. After applying the loading algorithm, the resulting margin will give the real gap and the related probability of error that can be achieved. Conversely, in other implementations LC-RA is more appropriate. For example in [16], LC-RA is adopted since direct modulation of DFB laser is implemented for a PON scenario. In [12], LC-MA is applied considering squared M QAM constellations. Here, the algorithm is adapted in order to take into account non-squared constellations by scaling the resulting energies of each subcarrier by a factor k_{MQAM}. When squared constellations are considered, the scaling factor is one. Alternatively, for non-squared constellations, the scaling factors are obtained taking as a reference the power of the QPSK format. Specifically, the normalized mean powers of the different modulation formats can be calculated according to [21]. Thus, the normalized mean power of BPSK ($\bar{P}_{BPSK}$) and 4 QAM format ($\bar{P}_{4QAM}$) are 1 and 2, respectively implying a power ratio of $\bar{P}_{BPSK}/\bar{P}_{4QAM} = 1/2$. On the other hand, the relation between both formats in terms of energy is $(2^{b_{BPSK}} - 1)/(2^{b_{4QAM}} - 1) = (2^1 - 1)/(2^2 - 1) = 1/3$, where b_{4QAM} and b_{BPSK} are the number of bits per symbols of the 4 QAM and BPSK formats, respectively. Hence, the scaling factor of BPSK format is $k_{BPSK} = 3/2$. Following this, the resulting scaling factors for 8 QAM, 32 QAM, and 128 QAM formats are $k_{8QAM} = 9/7$, $k_{32QAM} = 30/31$,

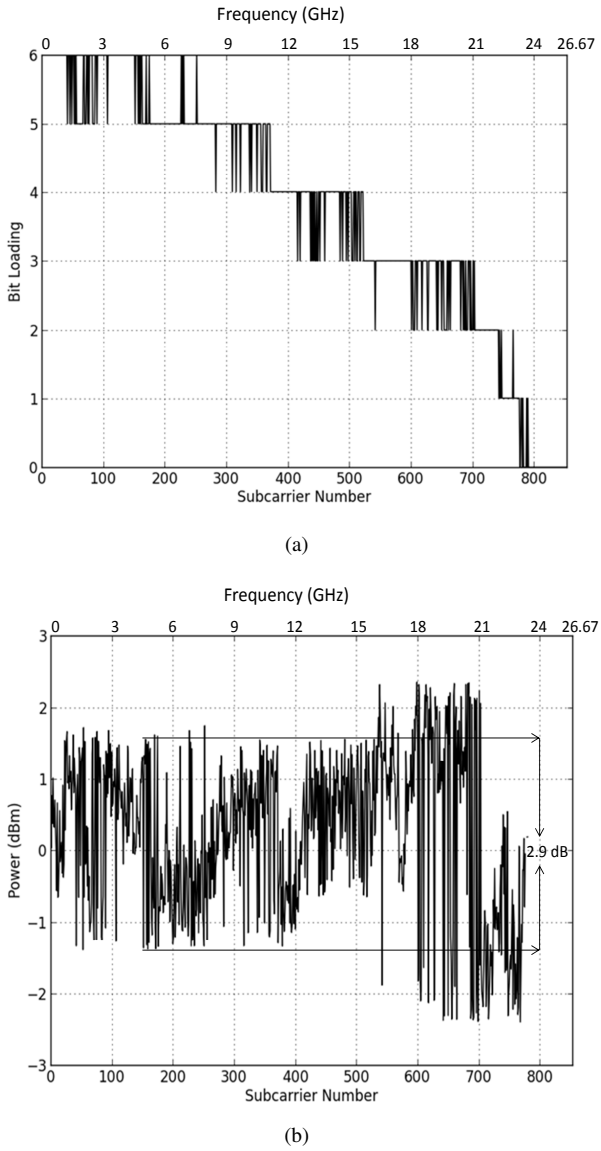

Fig. 5. (a) Bit loading and (b) power loading using LC-MA at 100 Gb/s in the B2B case.

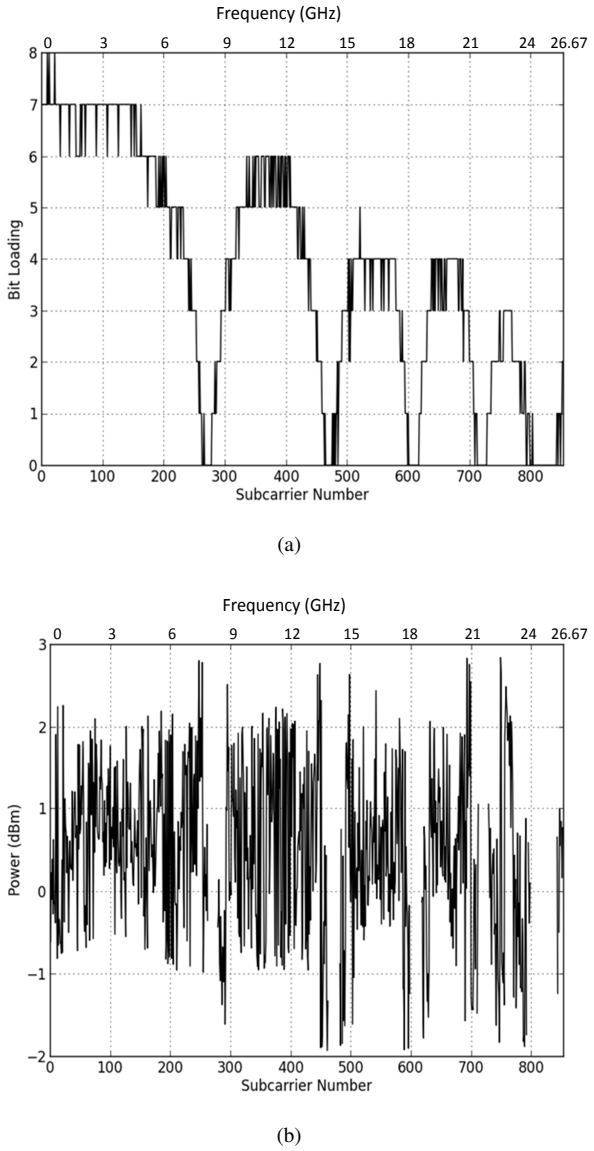

Fig. 6. (a) Bit loading and (b) power loading using LC-MA for 100 Gb/s after 50 km of SSMF.

and $k_{128QAM} = 123/127$, respectively. CCB algorithm is also implemented to solve the MA problem, for comparison with LC solution. In particular, CCB algorithm first computes the water-filling solution considering the SNR of the subcarriers, a tentative margin and Γ. Then, the resulting bit distribution is approximated by rounding the bit number values, according to the data rate constraint. As a last step, the energy is recalculated also including the scaling factors. It is worth mentioning that, if suboptimal CCB-MA is used in the transceiver DSP for reducing the computational complexity, the same parameters as in the LC case, namely the initial Γ and scaling factors, can be used.

Finally, in a real implementation, network information will be provided once at the beginning of the transmission. Since the optical channel changes very slowly, the latency due to the round trip for the CSI will not be a problem. Hence, latency will be related with the optical path setting. On the other hand, forward error correction (FEC) will also affect the latency as transmission delays for FEC encoding and decoding occur. Thus, different (FEC) schemes can be considered: hard decision FEC (HD-FEC), which has an overhead $\delta_{FEC} = 7\%$, and soft decision FEC (SD-FEC) with $\delta_{FEC} = 20\%$ [28], [29]. Depending on the used FEC coding scheme, a different target BER is allowed. Specifically, for the HD-FEC, the target BER is 10^{-3} [28]. Whereas SD-FEC gives a target BER of $1.9 \cdot 10^{-2}$ [30]. Additionally, other FEC can be used depending on latency and performance requirements [28], [31].

III. Performance analysis

In order to analyze the proposed DMT transponder described in section II and used in the system of Fig. 1, Python software is used. BPSK and M QAM formats are considered, with $M = 2^q$ and q variable between 2 and 9 according to the implemented loading algorithm (see Fig. 2)

[21]. 5 TS are added every 119 symbols to estimate the channel at the receiver side; 2 of them are also used for frame synchronization. Thus, the overhead due to the TS is 4%. The 124 DMT symbols are statistically independent and constitute a DMT frame which is repeatedly transmitted. As motivated in section II, an $N = 2048$ points IFFT is implemented considering that half of the subcarriers are used to force HS. A maximum of 852 subcarriers carry data in order to introduce an oversampling factor, $L = 1.2$, for avoiding aliasing in the filtering process. A CP of 1.56% is considered. Then, according to [25], the DMT signal is symmetrically clipped using a clipping level $C = 12$ dB. A model of the spectral behavior of a high speed CMOS 8 bits resolution DAC working at 64 GS/s is considered for digital-to-analog conversion [32]. Hence, the corresponding maximum DMT electrical signal bandwidth is 26.67 GHz ($B_s = \frac{64GS/s}{2 \cdot L}$). The optical carrier is set to 192.5 THz, and the MZM is biased at the quadrature point ($V_{bias}/V_\pi = -0.5$, where V_{bias} is the bias voltage and V_π the switching voltage). The peak-to-peak drive level has been adjusted to be about the 90% of V_π. The optical link is emulated with a SSMF (G.652). The split-step Fourier method is used to model the propagation over the SSMF with a dispersion coefficient of 17 ps/nm/km, a nonlinear coefficient of 1.37 $W^{-1}km^{-1}$ and 0.2 dB/km attenuation. The power at the input of the fiber is 5 dBm. ASE (amplified spontaneous emission) noise is modeled adding white optical noise. The OSNR is defined in a 12.5 GHz bandwidth. At the receiver, a variant of Schmidl & Cox's method is considered for frame synchronization, as defined in section II. One tap equalization with decision directed channel estimation is implemented. The BER is calculated using error counting. Bits are transmitted until at least 100 errors occur.

Considering a minimum FEC overhead of 7% and also taking into account the overhead due to CP and TS a total overhead of 13% is needed. When SD-FEC is implemented, the total overhead increases up to 26.7%. All the bit rates in the paper are gross data rates (R_g) which include the overhead due to FEC. The overhead due to CP and TS is not part of the gross data rate. Hence, the net data rates (R_n) can be calculated as $R_n = R_g/(1 + \delta_{FEC})$ according to [33].

In order to evaluate the system limitations, the SNR of each subcarrier is estimated in the B2B configuration by implementing decision directed channel estimation, as explained in section II. An initial channel estimation is performed by sending 5 TS and using uniform loading with 16 QAM format at 100 Gb/s. An OSNR of 31 dB is used in the estimation to limit the ASE noise influence and analyze other system impairments. In Fig. 3(a) it is shown that the 3 dB bandwidth of the DAC (13 GHz) is limiting the system, as the high frequency subcarriers present low values of SNR. In Fig. 3(b), the BER and number of errors per subcarrier is drawn for the B2B configuration. It can be observed that the last group of subcarriers presents more errors and high BER values, which causes the overall system performance degradation. In a second step, the same analysis is performed after 50 km of SSMF. Fig. 4(a) shows the channel estimation after 50 km of SSMF using 16 QAM format at 100 Gb/s. It can be seen that CD also limits the system performance. As a result various

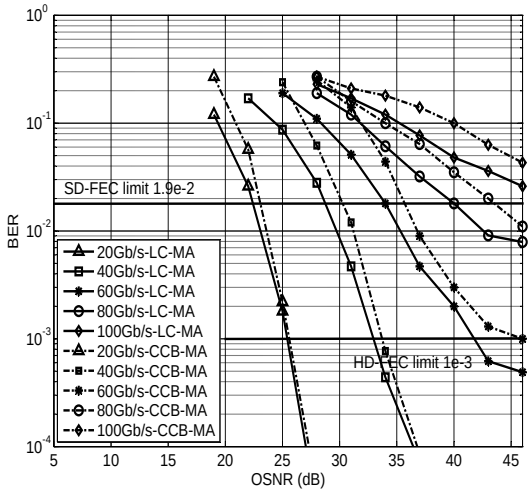

Fig. 7. BER performance comparison using LC-MA and CCB-MA algorithms vs OSNR for various bit rates after 50 km of SSMF.

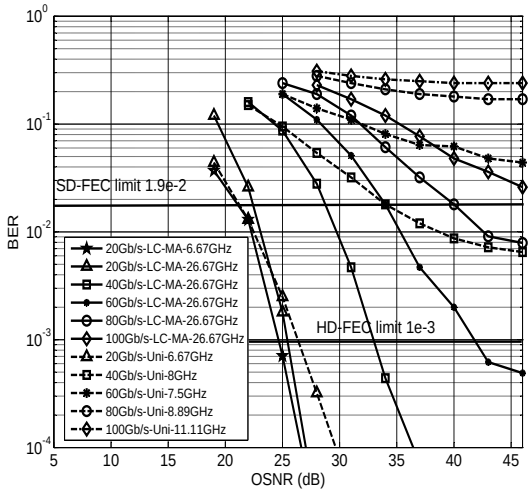

Fig. 8. BER performance comparison using LC-MA and uniform loading vs OSNR for various bit rates after 50 km of SSMF.

subcarriers are highly attenuated. According to equation (2), the first attenuation peak occurs around 8.53 GHz which correspond to the subcarrier 274. In Fig. 4(b) the number of errors and the BER per subcarrier after the fiber link are reported. It can be seen that the subcarriers affected by CD also present a high number of errors and BER values around 10^{-1}. In fact, each subcarrier suffers different power fading, depending on accumulated CD and the frequency of the subcarrier [34], [7]. It is shown that 100 Gb/s can not be transmitted, ensuring 10^{-3} BER, by using uniform loading for a DMT signal with 26.67 GHz bandwidth (neither in B2B configuration nor after 50 km of SSMF) due to system impairments that degrade the performance.

In order to asses the system impairments mitigation capability of LC-MA, this DSP functionality is applied to the system of Fig. 1. The resulting bit and power allocation, after applying LC-MA in a B2B configuration, can be seen

TABLE I
ACHIEVABLE REACH, REQUIRED OSNR FOR 10^{-3} BER, MAXIMUM ASSIGNED NUMBER OF BITS PER SYMBOL AND EFFECTIVE SIGNAL BANDWIDTH USING LC-MA AT DIFFERENT GROSS DATA RATES

Rate (Gb/s)	Reach (km)	OSNR (dB)	Max. # bits/symb	B_s (GHz) Effective
20	150	26	4	20.9
40	150	36	5	23.9
60	70	49	5	24.8
80	20	43	6	22.5
100	10	55	7	26.6

TABLE II
ACHIEVABLE REACH, f_{CD}^1, REQUIRED OSNR FOR 10^{-3} BER, SIGNAL BANDWIDTH AND MODULATION FORMAT USED TO IMPLEMENT UNIFORM LOADING AT DIFFERENT GROSS DATA RATES

Rate (Gb/s)	Reach (km)	f_{CD}^1 (GHz)	OSNR (dB)	B_s (GHz)	Format
20	140	5.1	40	4	32 QAM
40	40	9.5	41	8	32 QAM
60	20	13.5	47	10	64 QAM
80	10	19.1	40	16	32 QAM
100	0	24.3	40	20	32 QAM

in Fig. 5(a) and Fig. 5(b), respectively. In Fig. 5(a), it is shown that the first group of subcarriers, which present high values of SNR, are mapped with a 64 QAM format. It can also be seen that the modulation format order decreases with the reduction of the SNR. The last subcarriers that are affected by the DAC bandwidth limitation, do not carry data and their power is set to zero after applying LC-MA (see Fig. 5(b)). The change of the modulation format can also be seen in terms of power in Fig. 5(b). As an example, in Fig. 5(a), subcarrier 159 is mapped into a 32 QAM format, whereas subcarrier 160 is mapped into 64 QAM. According to [12] and considering the scaling factors of both formats (defined in section II), this change of modulation format corresponds to about 3 dB energy-gain. In fact, in Fig. 5(b) it can be observed that the power corresponding to subcarrier 159 and 160 varies from -1.4 dBm to 1.5 dBm, respectively. Finally, figures 6(a) and 6(b), show the bit and power loading distribution per subcarrier, respectively, after applying LC-MA considering a fiber link of 50 km of SSMF. It can be seen that the frequencies affected by CD do not carry data and hence, no power is assigned to these subcarriers. Power variation can also be seen in Fig. 6(b), corresponding to the change from one modulation format to another (see Fig. 6(a)).

In order to take into account both the DAC and CD effects, the BER performance of the proposed system of Fig. 1 is analyzed considering a SSMF link of 50 km. Firstly, LC-MA performance is compared with CCB-MA in order to show the superior performance over the suboptimal algorithm. In particular, Fig. 7 shows the BER performance using both loading algorithms. It can be seen, that LC-MA outperforms the CCB-MA algorithm in terms of required OSNR to achieve a target BER for all the analyzed cases. Specifically, applying LC-MA, a BER of 10^{-3} is ensured for 60 Gb/s with about 4 dB less OSNR than in CCB-MA case. Moreover, using LC-MA up to 80 Gb/s can be achieved for a target BER of $1.9 \cdot 10^{-2}$ given an OSNR of 40 dB. Whereas, 43 dB OSNR is needed to ensure the same data rate at this target BER after CCB-MA algorithm. For the rest of this paper the LC-MA algorithm is used to perform bit and power loading.

Fig. 8 shows the BER performance versus required OSNR using LC-MA evidencing the improvement over the uniform approach. For uniform loading at a fixed data rate, the modulation format and signal bandwidth combination is selected to require lowest OSNR at 10^{-3} target BER. The values are obtained through exhaustive simulations. Furthermore, B_s is chosen under the constraint of fixing a B_s lower than the frequency where the first attenuation peak due to CD (f_{CD}^1)

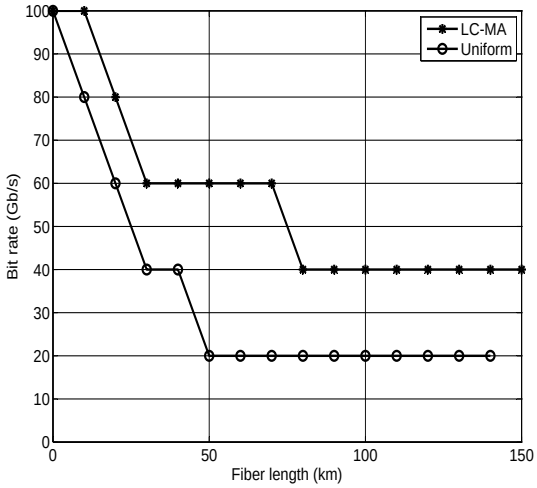

Fig. 9. Achievable data rate for a target BER of 10^{-3} using LC-MA algorithm and uniform loading for different fiber links.

appears. This value is updated for each fiber link. Hence, when a 50 km SSMF is considered, signal bandwidths lower than 8.53 GHz should be selected for uniform loading according to Fig. 4(a) and equation (2). As a result, in order to transmit at 20 Gb/s over 50 km of SSMF, and ensuring a target BER of 10^{-3}, a signal bandwidth of 6.67 GHz and 8 QAM modulation format for all subcarriers can be used requiring 26 dB OSNR. Other possibilities to achieve 20 Gb/s holding the 8.53 GHz maximum bandwidth restriction, could be 16 QAM with 5 GHz signal bandwidth or higher constellation formats with reduced signal bandwidths. However, these alternatives require a higher OSNR to ensure the same target BER of 10^{-3}. From Fig. 8, it can be seen that applying LC-MA with a $B_s = 26.67$ GHz at 20 Gb/s achieves better performance than uniform in the cases where a BER lower than 10^{-2} is obtained. In order to outperform uniform loading for any BER value, when a low data rate is transmitted, LC-MA should be applied with a reduced signal bandwidth. As a result, it is seen in Fig. 8 that transmitting at 20 Gb/s using the same bandwidth than in the uniform case, $B_s = 6.67$ GHz, LC-MA requires in all cases less OSNR than uniform loading to ensure the same target BER. On the other hand, in order to transmit at higher data rates, LC-MA is applied with a $B_s = 26.67$ GHz. Specifically, up to 60 Gb/s transmission is obtained using LC-MA ensuring a target BER of 10^{-3} with 42 dB OSNR. The same target BER can only be guaranteed up to 20 Gb/s when uniform loading is used. Considering a

BER threshold of $1.9 \cdot 10^{-2}$ up to 80 Gb/s can be transmitted using LC-MA with 40 dB OSNR. Conversely, with uniform loading up to 40 Gb/s transmission is achieved ensuring the same target BER of $1.9 \cdot 10^{-2}$ with 34 dB, $B_S = 8$ GHz and 32 QAM format.

Finally, in Fig. 9 the achievable data rate at 10^{-3} BER of the proposed transponder of Fig. 1 using LC-MA and the uniform loading scheme is analyzed for different fiber links. Data rate steps of 20 Gb/s are considered. Additionally, Table I shows the maximum achieved reach for different data rates, the required OSNR to ensure 10^{-3} BER, the maximum assigned number of bits per symbols per subcarrier and effective signal bandwidth according to LC-MA. Table II also includes the frequency of the first notch f_{CD}^1 and the optimum combinations of modulation format and signal bandwidth for a particular link at a fixed data rate. Please note that for 60 Gb/s, 64 QAM is the selected uniform format as the OSNR is minimized for a target BER of 10^{-3}. In fact, 60 Gb/s transmission using 32 QAM would be more affected by both CD and DAC bandwidth limitation, as a $B_s = 12$ GHz is required. A maximum link length of 150 km of SSMF has been considered, as long haul applications are not the target of the present work. From Fig. 9, it can be seen that with the increase of the fiber link LC-MA can transmit at a higher data rate than uniform loading for the same target BER of 10^{-3}. Specifically, LC-MA allows 100 Gb/s transmission over 10 km of SSMF ensuring a target BER of 10^{-3}, whereas with uniform bit and power loading 100 Gb/s can not be transmitted and in the B2B configuration an OSNR of 40 dB is required, considering a signal bandwidth of 20 GHz and 32 QAM format. Additionally, 20 Gb/s transmission is ensured after 140 km of SSMF with 40 dB OSNR and using uniform loading with a signal bandwidth of 4 GHz and the 32 QAM format. On the other hand, according to Fig. 9 and Table I, using LC-MA algorithm, the data rate is doubled for the same fiber link of 140 km, achieving 40 Gb/s transmission. Furthermore, this data rate can be maintained up to 150 km of SSMF with a required OSNR of 36 dB ensuring 10^{-3} BER and occupying an effective $B_s = 23.9$ GHz. Considering finer data rate steps of 10 Gb/s, the results presented in Fig. 10 have been obtained. It is shown that using LC-MA, up to 50 Gb/s can be transmitted over 150 km of SSMF at the same target BER with 41 dB OSNR. Also 80 km of SSMF has been considered in the analysis of Fig. 10, as it is a possible extended reach for data center connections. In particular, 50 Gb/s can be transmitted over 80 km of SSMF ensuring a target BER of 10^{-3} with about 37 dB OSNR. As latency is also related to the adopted FEC scheme, using a simpler FEC coding with 10^{-4} target BER, such as the Reed-Solomon RS(255,239) code, the system latency can be reduced [31]. Considering this target BER, up to 40 Gb/s can be transmitted over 80 km of SSMF with 39 dB OSNR.

IV. Experimental and numerical comparison

Fig. 11 shows the set-up that has been used for experimental assessment of the proposed transponder [20]. The signal processing has been performed offline using Python software.

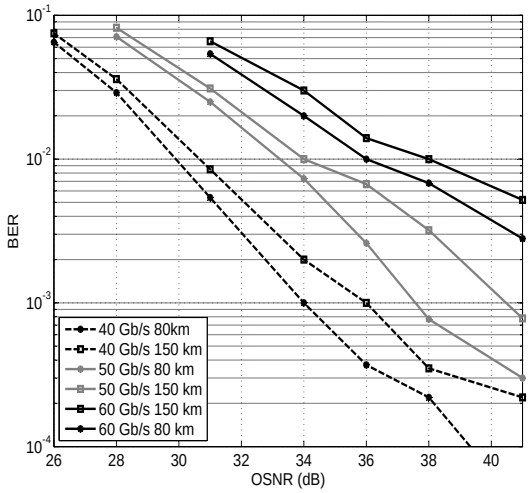

Fig. 10. BER performance using LC-MA vs OSNR for 40 Gb/s, 50 Gb/s and 60 Gb/s after 80 km and 150 km of SSMF.

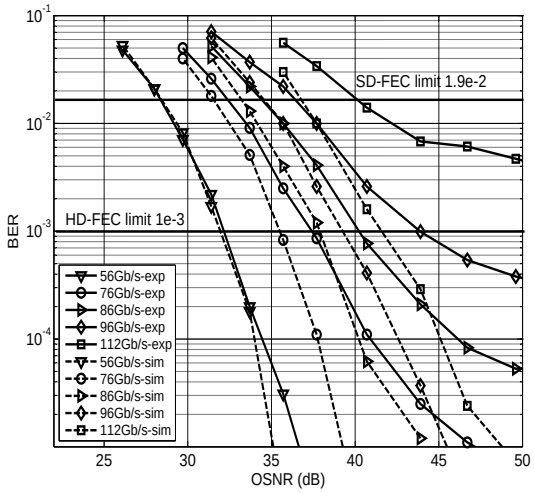

Fig. 12. Experimental and numerical BER curves for different data rates and OSNR values in the B2B configuration.

Tx and Rx DSP modules are the same used in simulation (as described in section II). A commercial 8 bits resolution DAC running at 64 GS/s has been used for the experimental validation [32]. A signal bandwidth of 26.67 GHz is considered and the optical carrier is set to 192.5 THz. The MZM is biased at the quadrature point and it is suited for 40 GHz bandwidth signals. A single span of SSMF of 50.5 km and 82.1 km with 0.2 dB/km attenuation is used. The launch power into the SSMF is set to 5 dBm. Erbium doped fiber amplifiers (EDFA) are added to the system to perform OSNR measurements. In order to measure high OSNR values only the inline EDFA is needed, whereas to achieve low values of OSNR a second EDFA (dashed box in Fig. 11) is added for additional noise loading. The OSNR is defined in a 12.5 GHz bandwidth. A bandpass filter of 100 GHz bandwidth is used to limit the ASE noise for optical-to-electrical conversion. For reception, a 50 GHz PIN photodiode is used and its input power is at

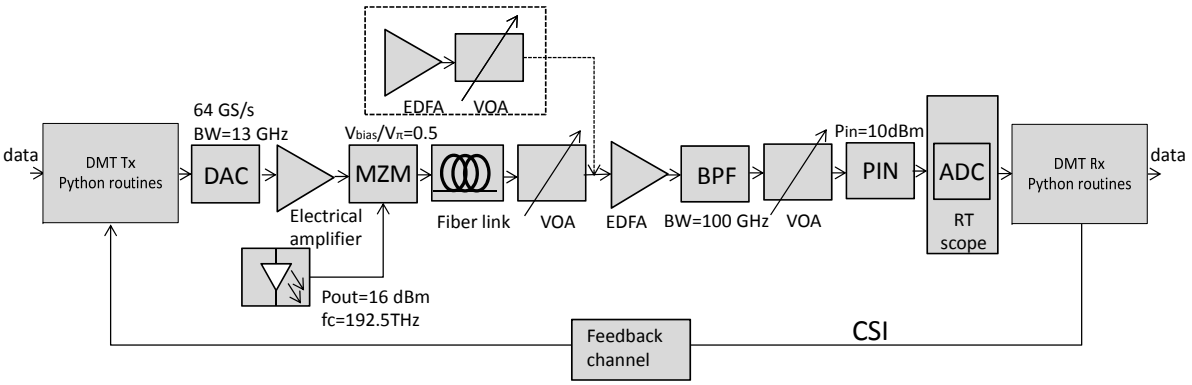

Fig. 11. Experimental set-up.

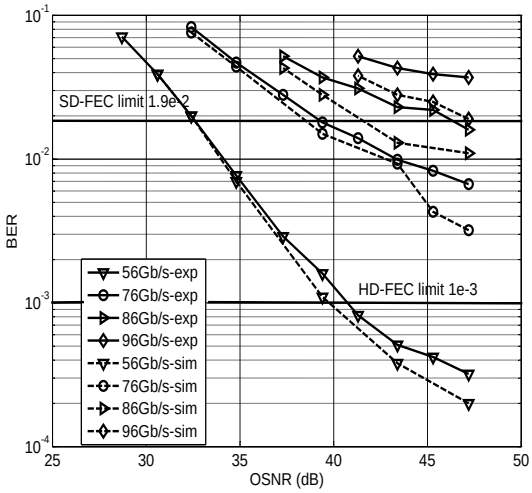

Fig. 13. Experimental and numerical BER curves for different data rates and OSNR values after 50.5 km of SSMF.

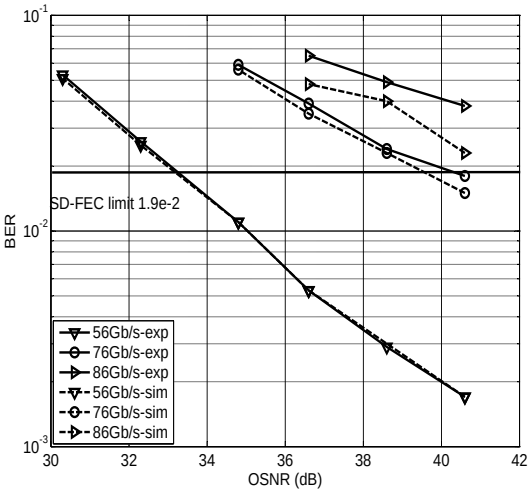

Fig. 14. Experimental and numerical BER curves for different data rates and OSNR values after 82.1 km of SSMF.

10 dBm using variable optical attenuators (VOA). Taking into account the required maximum effective B_S, a PIN with lower bandwidth can be used. For example in [16], an 8.4 GHz APD is adopted. The photodetected signal is captured by an 80 GS/s real-time oscilloscope with 29.4 GHz bandwidth. The SNR per subcarrier is estimated for each value of OSNR in order to perform the loading algorithm.

In Fig. 12, the experimental results [20] are compared to the numerical BER curves of the proposed adaptive DMT transponder using LC-MA algorithm vs the OSNR in a B2B system configuration. It can be seen that up to 96 Gb/s is experimentally achieved (considering a target BER of 10^{-3}) for 44 dB OSNR. Hence, high data rates are achieved using LC-MA algorithm, but at the expense of a high OSNR requirement. In case of using an increased overhead, 112 Gb/s is experimentally achieved with 40 dB OSNR for a target BER of $1.9 \cdot 10^{-2}$. Using a simpler FEC scheme, 86 Gb/s is experimentally demonstrated at 10^{-4} BER. In general, lower OSNR values are required in simulation to achieve a certain target BER, when comparing with experimental results. The difference between experimental and simulation curves becomes higher for the increasing data rate. This effect is mainly due to the fact that in the experiments the nonlinearity impairments caused by the electronic and optoelectronic devices, such as the MZM, the drivers and the effective number of bits (ENOB) of the converters, highly degrade the system performance especially when high order constellations are used. Additional experiments have been performed in order to analyze the system robustness against CD and evaluate the BER performance of the proposed adaptive transponder considering 50.5 km and 82.1 km of SSMF as possible extended links suitable for inter data center connections. Fig. 13 shows the obtained BER curves at data rates varying between 56 Gb/s and 96 Gb/s after 50.5 km of SSMF for different OSNR values. Considering HD-FEC, 56 Gb/s gross data rate (which corresponds to a net data rate of 52.3 Gb/s) is transmitted. Specifically, the OSNR requirement for this data rate to ensure a BER of 10^{-3} is 41 dB OSNR (1 dB more than in simulation), as it can be seen in Fig. 13. Considering a target BER of $1.9 \cdot 10^{-2}$, up to 86 Gb/s is transmitted over 50.5 km of fiber with an OSNR of 46 dB. Fig. 14 shows the BER performance for different data rates after a

longer SSMF distance of 82.1 km. At that distance, 56 Gb/s transmission cannot be achieved for a target BER of 10^{-3} with the analyzed OSNR values. However, using a different code to implement HD-FEC with 7% overhead, such as two interleaved extended BCH(1020,988), $4 \cdot 10^{-3}$ BER can be considered according to [28]. At this BER value, 56 Gb/s can be successfully transmitted with 37 dB OSNR as numerically and experimentally demonstrated in Fig. 14. Moreover, with an OSNR of 40 dB up to 76 Gb/s can be experimentally transmitted for $1.9 \cdot 10^{-2}$ target BER. In these last analysis, where the fiber link is considered, simulations are closer to experiments as the chromatic dispersion dominates over the MZM nonlinearities.

V. Conclusion

A cost-effective DMT transponder with adaptive loading capabilities has been designed using a DD optical setup. Simulations show that, using loading schemes system impairments such as fiber CD and DAC bandwidth limitations are mitigated enabling high data rate transmission over short range fiber links. The LC-MA solution outperforms the CCB-MA loading algorithm in terms of required OSNR for a fixed target BER. At the same time, the LC-MA scheme achieves higher data rate and reach compared with bandwidth variable uniform loading optimized according to the transmission impairments. 50 Gb/s can be transmitted beyond 80 km of SSMF, enabling high data rate transmission over an extended link reach between data centers. Additionally, reducing the gross data rate, longer inter data center connections can be covered. The experimental assessment of the designed transponder demonstrates up to 56 Gb/s optical DMT transmission over 82.1 km of SSMF. Hence, it is demonstrated that the provided guidelines allow designing adaptive cost-effective transponders enabling a possible extension of data center interconnections.

References

[1] C. Cole, "Beyond 100G client optics," *IEEE Comm. Magaz.*, vol. 50, no. 2, pp. 58–66, 2012.

[2] Cisco, "Cisco global cloud index: Forecast and methodology, 2012-2017," *Cisco white paper*, 2013.

[3] S. Gringeri, E. Basch, and T. Xia, "Technical considerations for supporting data rates beyond 100 Gb/s," *IEEE Comm. Magaz.*, vol. 50, no. 2, pp. 21–30, 2012.

[4] C. Cole, I. Lyubomirsky, A. Ghiasi, and V. Telang, "Higher-order modulation for client optics," *IEEE Comm. Magaz.*, vol. 51, no. 3, pp. 50–57, 2013.

[5] P. Winzer, "Beyond 100G Ethernet," *IEEE Comm. Magaz.*, vol. 48, no. 7, pp. 26–30, 2010.

[6] W. Shieh and I. Djordjevic, *OFDM for Optical Communications*. Elsevier, 2010.

[7] D. Barros and J. Kahn, "Comparison of orthogonal frequency-division multiplexing and on-off keying in amplified direct-detection single-mode fiber systems," *J. of Lightw. Technol.*, vol. 28, no. 12, pp. 1811–1820, 2010.

[8] S. C. J. Lee, F. Breyer, S. Randel, H. P. A. van den Boom, and A. M. J. Koonen, "High-speed transmission over multimode fiber using discrete multitone modulation," *J. Opt. Netw.*, vol. 7, no. 2, pp. 183–196, 2008.

[9] M. Svaluto Moreolo, R. Munoz, and G. Junyent, "Novel power efficient optical OFDM based on hartley transform for intensity-modulated direct-detection systems," *J. Lightw. Technol.*, vol. 28, no. 5, pp. 798 –805, 2010.

[10] D. Torrientes, P. Chanclou, F. Laurent, S. Tsyier, Y. Chang, B. Charbonnier, and C. Kazmierski, "10Gbit/s for next generation PON with electronic equalization using un-cooled 1.55 μm directly modulated laser," in *European Conf. on Opt. Comm.(ECOC)*, 2009.

[11] B. Lin, J. Li, H. Yang, Y. Wan, Y. He, and Z. Chen, "Comparison of DSB and SSB transmission for OFDM-PON," *J. of Opt. Comm. and Netw.*, vol. 4, no. 11, pp. 94–100, 2012.

[12] J. Cioffi, "Data transmission theory, chapter 4 of course text for EE379A-B and EE479," *Stanford University*. [Online]. Available: www.stanford.edu/group/cioffi/book/

[13] H. Paul and K. D. Kammeyer, "Subcarrier selection for IM/DD OFDM systems," in *European Conf. on Opt. Comm. (ECOC)*, 2009, p. P3.11.

[14] R. F. H. Fischer and J. Huber, "A new loading algorithm for discrete multitone transmission," in *Communications: The Key to Global Prosperity Global Telecommunications Conference, GLOBECOM*, vol. 1, Nov 1996, pp. 724–728.

[15] G. Gallager, *Information Theory and Reliable Communication*. Wiley, 1969.

[16] C. Milion, T. Duong, N. Genay, E. Grard, V. Rodrigues, B. Charbonnier, J. Le Masson, M. Ouzzif, P. Chanclou, and A. Gharba, "High bit rate transmission for NG-PON by direct modulation of DFB laser using discrete multi-tone," in *European Conf. on Opt. Comm.(ECOC)*, Sept 2009, p. 7.5.4.

[17] T. Tanaka, M. Nishihara, T. Takahara, L. Li, Z. Tao, and J. Rasmussen, "50 Gbps class transmission in single mode fiber using discrete multitone modulation with 10G directly modulated laser," in *Opt. Fiber Comm. Conf. and Exp. and the National Fiber Optic Engineers Conf. (OFC/NFOEC)*, 2012.

[18] W. Yan, T. Tanaka, B. Liu, M. Nishihara, L. Li, T. Takahara, Z. Tao, J. Rasmussen, and T. Drenski, "100 Gb/s optical IM-DD transmission with 10G-class devices enabled by 65 GS/s CMOS DAC core," in *Opt. Fiber Comm. Conf. and Exp. and the National Fiber Optic Engineers Conf. (OFC/NFOEC)*, 2013.

[19] B. Schmidt, A. Lowery, and J. Armstrong, "Experimental demonstrations of electronic dispersion compensation for long-haul transmission using direct-detection optical OFDM," *J. of Lightw. Technol.*, vol. 26, no. 1, pp. 196–203, 2008.

[20] A. Dochhan, L. Nadal, H. Griesser, M. Eiselt, M. Svaluto Moreolo, and J. P. Elbers, "Experimental investigation of discrete multitone transmission in the presence of optical noise and chromatic dispersion," in *Opt. Fiber Comm. Conf. (OFC)*, 2014, p. Tu2G.7.

[21] J. G. Proakis and M. Salehi, *Digital Communications*. McGraw-Hill Higher Education, 2007.

[22] H. Takahashi, A. Al Amin, S. Jansen, I. Morita, and H. Tanaka, "Highly spectrally efficient DWDM transmission at 7.0 b/s/Hz using 8x65.1-gb/s coherent PDM-OFDM," *J. of Lightw. Technol.*, vol. 28, no. 4, pp. 406–414, Feb 2010.

[23] L. Nadal, M. Svaluto Moreolo, J. M. Fabrega, and G. Junyent, "Clipping and quantization noise mitigation in intensity-modulated direct detection O-OFDM systems based on the FHT," in *Int. Conf. Transp. Opt. Netw.*, 2012.

[24] S. Randel, F. Breyer, S. C. J. Lee, and J. Walewski, "Advanced modulation schemes for short-range optical communications," *IEEE J. of Selected Topics in Quantum Electr.*, vol. 16, no. 5, pp. 1280–1289, Sept 2010.

[25] E. Vanin, "Performance evaluation of intensity modulated optical OFDM system with digital baseband distortion," *Opt. Exp.*, vol. 19, no. 5, pp. 4280–4293, 2011.

[26] T. Schmidl and D. Cox, "Robust frequency and timing synchronization for OFDM," *IEEE Tran. on Comm.*, vol. 45, no. 12, pp. 1613–1621, 1997.

[27] P. Chow, J. Cioffi, and J. A. C. Bingham, "A practical discrete multitone transceiver loading algorithm for data transmission over spectrally shaped channels," *IEEE Tran. on Comm.*, vol. 43, no. 234, pp. 773–775, 1995.

[28] "ITU-T recommendation G.975.1," 2004.

[29] T. Mizuochi, Y. Konishi, Y. Miyata, T. Inoue, K. Onohara, S. Kametani, T. Sugihara, K. Kubo, T. Kobayashi, H. Yoshida, and T. Ichikawa, "Fpga based prototyping of next generation forward error correction," in *European Conf. on Opt. Comm. (ECOC)*, 2009.

[30] G. Zhang, L. Nelson, Y. Pan, M. Birk, C. Skolnick, C. Rasmussen, M. Givehchi, B. Mikkelsen, T. Scherer, T. Downs, and W. Keil, "3760km, 100G SSMF transmission over commercial terrestrial DWDM ROADM systems using SD-FEC," in *Opt. Fiber Comm. Conf. and Exp. and the National Fiber Optic Engineers Conf. (OFC/NFOEC)*, March 2012, pp. 1–3.

[31] "ITU-T recommendation G.975," 2000.

[32] Fujitsu, "Leia 55 65 GSa/s 8-bit DAC," *Fact sheet*. [Online]. Available: http://www.fujitsu.com/downloads/MICRO/fme/documentation/c60.pdf

[33] S. L. Jansen, B. Spinnler, I. Morita, S. Randel, and H. Tanaka, "100GbE: QPSK versus OFDM," *Opt. Fib. Technol.*,

vol. 15, no. 56, pp. 407 – 413, 2009. [Online]. Available: http://www.sciencedirect.com/science/article/pii/S1068520009000522

[34] L. Bangjiang, L. Juhao, Y. Hui, W. Yangsha, H. Yongqi, and C. Zhangyuan, "Comparison of DSB and SSB transmission for OFDM-PON," *J. Opt. Commun. Netw.*, vol. 4, no. 11, pp. 94–100, Nov. 2012.